Gastroenterology Report, 2024, **12**, goae087
https://doi.org/10.1093/gastro/goae087
Original Article

Original Article

Strain- and sex-specific differences in intestinal microhemodynamics and gut microbiota composition

Sunjing Fu[1,2], Mengting Xu[1,2], Bing Wang[1,2], Bingwei Li[1,2], Yuan Li[1,2], Yingyu Wang[1,2], Xueting Liu[1,2], Hao Ling[3], Qin Wang[1,2], Xiaoyan Zhang[1,2], Ailing Li[1,2], Xu Zhang[4] and Mingming Liu [1,2,5,*]

[1]Institute of Microcirculation, Chinese Academy of Medical Sciences & Peking Union Medical College, Beijing, P. R. China
[2]International Center of Microvascular Medicine, Chinese Academy of Medical Sciences & Peking Union Medical College, Beijing, P. R. China
[3]Department of Radiology, The Affiliated Changsha Central Hospital, Hengyang Medical School, University of South China, Changsha, Hunan, P. R. China
[4]Laboratory of Electron Microscopy, Ultrastructural Pathology Center, Peking University First Hospital, Beijing, P. R. China
[5]Diabetes Research Center, Chinese Academy of Medical Sciences & Peking Union Medical College, Beijing, P. R. China

*Corresponding author. Institute of Microcirculation, Chinese Academy of Medical Sciences & Peking Union Medical College (CAMS & PUMC), No.5 Dong Dan Third Alley, Dongcheng District, Beijing 100005, China. Email: mingmingliu@imc.pumc.edu.cn

Abstract

Background: Intestinal microcirculation is a critical interface for nutrient exchange and energy transfer, and is essential for maintaining physiological integrity. Our study aimed to elucidate the relationships among intestinal microhemodynamics, genetic background, sex, and microbial composition.

Methods: To dissect the microhemodynamic landscape of the BALB/c, C57BL/6J, and KM mouse strains, laser Doppler flowmetry paired with wavelet transform analysis was utilized to determine the amplitude of characteristic oscillatory patterns. Microbial consortia were profiled using 16S rRNA gene sequencing. To augment our investigation, a broad-spectrum antibiotic regimen was administered to these strains to evaluate the impact of gut microbiota depletion on intestinal microhemodynamics. Immunohistochemical analyses were used to quantify platelet endothelial cell adhesion molecule-1 (PECAM-1), estrogen receptor α (ESR1), and estrogen receptor β (ESR2) expression.

Results: Our findings revealed strain-dependent and sex-related disparities in microhemodynamic profiles and characteristic oscillatory behaviors. Significant differences in the gut microbiota contingent upon sex and genetic lineage were observed, with correlational analyses indicating an influence of the microbiota on microhemodynamic parameters. Following antibiotic treatment, distinct changes in blood perfusion levels and velocities were observed, including a reduction in female C57BL/6J mice and a general decrease in perfusion velocity. Enhanced erythrocyte aggregation and modulated endothelial function post-antibiotic treatment indicated that a systemic response to microbiota depletion impacted cardiac amplitude. Immunohistochemical data revealed strain-specific and sex-specific PECAM-1 and ESR1 expression patterns that aligned with observed intestinal microhemodynamic changes.

Conclusions: This study highlights the influence of both genetic and sex-specific factors on intestinal microhemodynamics and the gut microbiota in mice. These findings also emphasize a substantial correlation between intestinal microhemodynamics and the compositional dynamics of the gut bacterial community.

Keywords: intestinal microhemodynamics; mouse strains; sex differences; gut microbiota; wavelet transform

Introduction

The gastro-intestinal microenvironment is a complex and dynamically orchestrated milieu that is central to the regulation of homeostatic functions within the body. The intestinal microcirculation, comprising a dense labyrinth of microvasculature and capillaries, is pivotal for facilitating nutrient uptake and the exchange of metabolic intermediates [1]. This microvascular network also serves as a sentinel, guarding the luminal interface against the ingress of deleterious substances and pathogenic microorganisms [2]. The governance of these microvessels is subject to a tightly regulated array of neural and humoral stimuli in which the communication of nutritional elements and endocrine signals orchestrates vascular responsiveness [3]. The subtleties of microhemodynamics within this context are crucial for ensuring effective tissue oxygenation and the equitable distribution of nutrients, which are indispensable for cellular metabolism and function [4]. Disruptions in intestinal microcirculatory processes have been implicated in the etiology of an extensive spectrum of pathological conditions [5, 6], signifying the importance of maintaining microvascular integrity for optimal gastro-intestinal function.

Scientific inquiry into sex-specific physiological variations has burgeoned [7], revealing disparities that have critical implications for disease manifestation and therapeutic approaches. The hypothesis that the metabolic requirements of males and females within a species precipitate differential adaptations in their respective microvascular architectures is not without merit [8]. This posited sexual dimorphism in microvascular function is supported by the delineation of distinct sex-based microbiomic profiles, which are known to exert a significant modulatory effect

Received: 15 December 2023. **Revised:** 30 June 2024. **Accepted:** 06 August 2024

on the structure and functionality of the intestinal vasculature [9, 10]. These microbiomic variances have been posited as potential contributing factors to the sex-specific prevalence of certain gastro-intestinal disorders, including but not limited to inflammatory bowel disease and irritable bowel syndrome [11–13].

Laser Doppler flowmetry (LDF) has emerged as a sophisticated and non-invasive technique for the real-time assessment of microvascular blood flow, exploiting the Doppler shift of monochromatic laser light as it scatters from moving red blood cells [14]. The complexity inherent in LDF signal profiles is reflective of the multiscale temporal variations and is influenced by a multitude of physiological parameters, encompassing cardiac contractions, respiratory movements, myogenic vessel wall activities, neurogenic stimuli, and endothelium-dependent modulations [15]. The integration of wavelet analytical methodologies with LDF has been instrumental in disentangling these complex signal patterns [16], providing a more refined understanding of the discrete components that contribute to the overall microhemodynamic milieu. The current study aims to investigate the interdependencies between genetic factors specific to mouse strains and the physiological distinctions associated with sex by assessing their impacts on intestinal microhemodynamics.

Methods and materials

Animals

The animal experiments performed in this study conformed to ethical standards and regulatory frameworks. In alignment with these guidelines, the experimental protocols of the present study were reviewed and approved by the Institutional Animal Care and Use Committee of the Institute of Microcirculation at the Chinese Academy of Medical Sciences (CAMS), adhering to the Principles and Guidelines for the Care and Use of Laboratory Animals (CAMS-IM-IACUC-2022-AE-0608).

For this investigation, 8-week-old murine specimens from the BALB/c, C57BL/6J, and KM strains were acquired from Vital River Laboratory Animal Technology (Beijing, China) and each cohort consisted of six mice. The animals were subsequently allocated to distinct housing units with meticulously controlled environmental conditions that featured a 12-h light–dark photoperiod, a stable temperature of 26°C, and a humidity range that was maintained at between 55% and 70%. The mice were afforded ad libitum access to standard laboratory chow and water throughout the study.

Blood pressure measurement

Blood pressure—a critical physiological parameter—was measured by using an Intelligent Noninvasive Sphygmomanometer BP-2010A (Softron Biotechnology, Beijing, China). The mice were acclimated within restraint apparatus that was positioned atop a thermally regulated surface preset to 37°C. The occlusion tail cuff was affixed to the sensor (BP98-RCP-M; Softron Biotechnology) and, following a 5-min acclimatization interval, the systolic, diastolic, and mean arterial blood pressures were recorded. To ensure accuracy, each measurement was obtained in triplicate.

Determination of the intestinal microhemodynamics

Intestinal microcirculatory parameters were determined by using a Moor VMS-LDF2 (Moor Instruments, Axminster, UK). After 30 min of acclimation, the mice were anesthetized by inhaling 2% isoflurane (R510-22; RWD Life Science Co., Shenzhen, Guangdong, China) in a 50% oxygen mixture using a small animal anesthesia machine (matrix VMR; Midmark Corporation, OH, USA). The intestine was gently exposed through a median incision and the VP4 probe was stably positioned on the exposed intestinal tissue. Three sites were selected and measured for 1 min each, and the backscattered light collected by the probe was processed by analog and digital signals to generate intestinal microhemodynamics. After the measurements, all the mice were sacrificed by cervical dislocation. The average blood perfusion rate was calculated as the amount of microvascular blood perfusion divided by time (min) and the velocity was determined based on the changes in the scattered light intensity of standard microparticles. Furthermore, the number of peaks that occurred each minute and the difference in perfusion units (ΔPUs) between the minimum and highest PUs were used to quantify the frequency and amplitude of microvascular vasomotion, respectively. Additionally, the distribution pattern was generated based on the level of microcirculatory blood perfusion.

Wavelet transform spectral analysis

The combination of LDF with wavelet transform can be used to assess microcirculatory dynamics related to physiological phenomena. Accordingly, the wavelet transform was utilized to transform microhemodynamic signals into the time–frequency domain, revealing the contributions of biological oscillators to changes in microcirculation. The frequency spectrum was divided into several spectra that corresponded to nitric oxide (NO)-independent and NO-dependent endothelial, neurogenic, myogenic, respiratory, and cardiac oscillators at frequencies of 0.005–0.0095, 0.0095–0.04, 0.04–0.15, 0.15–0.4, 0.4–2, and 2–5 Hz, respectively. Based on the microhemodynamic spectrum, the Morlet wavelet was scaled to generate a Gaussian window that was shifted along the time and frequency domains, and spectral amplitudes were determined by averaging the wavelet coefficients. Therefore, a 3D amplitude spectral scalogram of the wavelet-transformed microhemodynamic data was constructed. The coordinates contained variations in time (s), frequency (Hz), and spectral amplitude (AU). The amplitudes of the six oscillators were compared among female and male BALB/c, C57BL/6J, and KM mice.

Histology and immunohistochemistry

For morphological studies, tissues were fixed with 4% paraformaldehyde, embedded in paraffin, and cut into 5-μm-thick slices for hematoxylin and eosin (H&E) and immunohistochemical staining. For antigen retrieval, the slices were deparaffinized, rehydrated, and incubated in 10 mM of boiling citrate buffer (pH = 6.0; Zhongshan Golden Bridge Biotechnology, Beijing, China). The sections were then incubated with 3% hydrogen peroxide to inhibit endogenous peroxidase activity and blocked with 3% bovine serum albumin (BSA; TBD Science Technology, Tianjin, China) in phosphate-buffered saline. The sections were incubated in blocking buffer overnight at 4°C after incubation with primary mouse monoclonal antibodies against PECAM-1 (1:100; Santa Cruz Biotechnology, Dallas, TX, USA) or anti-mouse ESR1 and ESR2 monoclonal antibodies (1:25; Abcam, Waltham, MA, USA). Next, the samples were incubated in horseradish peroxidase-conjugated secondary antibodies (Zhongshan Golden Bridge) and 3,3'-diaminobenzidine tetrahydrochloride solution (Zhongshan Golden Bridge), dehydrated, and mounted. Finally, positive staining was detected by using a Leica DFC450 microscope (Leica Microsystems, Leitz, Germany). For quantitative evaluation, ImageJ software (National Institutes of Health, Bethesda, MD, USA) with a plug-in named "IHC profiler" was used to capture and analyse the digital images of the stained sections. In addition, the intensity of PECAM-1-, ESR1-, and ESR2-positive staining and the percentage of positive cells were quantified by calculating the integrated density.

16S rRNA gene sequence analysis

A QIAamp® DNA Stool Mini Kit (Qiagen, Hilden, Germany) was used to extract microbial DNA from the fecal samples. Polymerase chain reaction (PCR) was used to amplify the V3-V4 hypervariable sections of the bacterial 16S rRNA gene with the primers 338F (5′-ACTCCTACGGGAGGCA
GCAG-3′) and 806R (5′-GGACTACHVGG GTWTCTAAT-3′). PCRs were performed in triplicate with 20-μL mixtures. An Agencourt AMPure XP Kit (Beckman Coulter, Brea, CA, USA) was used to purify the amplicons after extraction from 1% agarose gels. The V3 and V4 regions from the 16S rRNA gene were amplified and purified as described previously. Following that, equimolar amounts of purified amplicons were pooled and paired-end sequenced on an Illumina MiSeq platform (Illumina, San Diego, CA, USA). Trimmomatic and Pear were used to quality-filter the raw FastQ files before merging them with Flash and Pear. Based on known database comparisons, low-quality and undesirable sequences were removed and finally analysed using QIIME.

ABX mice models

To elucidate the role of the gut microbiota in intestinal microhemodynamics, we further utilized mice subjected to a broad-spectrum antibiotic regimen that involved three genetically diverse mouse strains, each represented by both male and female subjects, with six individuals per sex per strain. The mice underwent a 3-day course of oral gavage, with each mouse receiving 200 μL of an antibiotic cocktail daily. This cocktail was composed of ampicillin, gentamicin, metronidazole, neomycin, and vancomycin, each at a concentration of 1 mg/mL, except for vancomycin, which was administered at 0.5 mg/mL. This composition and the dosing regimen are consistent with protocols outlined in a previous study [17]. Post-treatment, all mice were housed under specific pathogen-free conditions. This environment was strictly controlled and featured the same 12-h light–dark cycle. Additionally, both water and chow were autoclaved to prevent any inadvertent microbial contamination until the intestinal microhemodynamics were determined.

Statistical analysis

The statistical analysis was performed by using GraphPad Prism software (version 8.02; GraphPad Software, Inc., CA, USA). The data that were derived from laser Doppler signals and wavelet analysis are presented as the mean ± standard error of the mean (SEM). The Student's *t*-test and two-way analysis of variance (ANOVA) were employed to discern the differences in the parameters of interest across multiple groups, with the Tukey post hoc test applied to ANOVA for pairwise comparisons. The statistical significance threshold was established at a $P < 0.05$. Furthermore, to explore the relationships between the bacterial genera and the intestinal microhemodynamics indices, Spearman correlation analysis was conducted.

Results

Sex- and strain-dependent variations in baseline physiological parameters

The baseline characteristics of the studied mouse strains are shown in Table 1. At 8 weeks old, male mice consistently exhibited greater body weights than did their female counterparts. Compared with male mice, female mice exhibited elevated heart rates, with significant sexual variations observed in the BALB/c strain. Additionally, males exhibited increased diastolic blood pressure and mean arterial pressure levels across all groups. Analysis of pulse pressure revealed reduced differentials in females compared with males within the BALB/c and C57BL/6J strains. No significant differences in systolic blood pressure, diastolic blood pressure, or mean arterial pressure were detected between the sexes in the C57BL/6J and KM strains.

Sex-specific expression of vascular and hormonal markers in intestinal tissues

We quantified the number of villi and microvessels in the mucosal layer to assess vascular density across different mouse strains (Figure 1A). The ratio of villi to blood vessels was lower in female C57BL/6J mice than in female BALB/c and male C57BL/6J mice. In addition, blood microvessels from male C57BL/6J and KM mice displayed a more clustered distribution within the mucosal layer. Conversely, the other groups exhibited a relatively dispersed distribution of blood vessels in the mucosal layer. Immunohistochemical staining of the intestine revealed PECAM-1 expression on both the luminal surfaces and within the microvascular compartments of the microvilli (Figure 1B). ESR1 and ESR2 staining was predominantly observed in parts of the microvilli (Figure 1C). Semi-quantitative immunohistochemical analysis revealed that the proportion of PECAM-1-reactive cells was significantly greater in the intestines of female BALB/c mice than in those of male and female C57BL/6J mice; however, no significant differences in expression levels were observed among the other groups. Regarding ESR1, male C57BL/6J mice displayed a significantly greater percentage of positive cells than their female counterparts and KM males, and male BALB/c mice exhibited a significantly higher proportion of cells with ESR1 reactivity than female BALB/c mice. As for staining intensity, male BALB/c mice were lower than female BALB/c mice ($P < 0.05$), suggesting strain- and sex-specific regulation of this receptor. In contrast, ESR2 expression levels did not differ

Table 1. Baseline characteristics of different mouse strains and sexes

	BALB/c		C57BL/6J		KM	
	Female	Male	Female	Male	Female	Male
Weight (g)	18.53 ± 0.33	21.62 ± 0.13[a]	18.03 ± 0.26[b]	27.23 ± 0.44[a,b]	30.75 ± 0.55[c]	37.00 ± 0.62[ab,c]
HR (bpm)	491.83 ± 8.03	572.33 ± 7.86[a]	672.33 ± 7.85[b]	684.83 ± 5.34[b]	531.17 ± 12.19[bc]	558.33 ± 13.28[b]
SBP (mmHg)	115.50 ± 1.71	115.67 ± 1.05	102.50 ± 2.08[b]	106.5 ± 0.81[b]	106.17 ± 1.08[b]	107.17 ± 3.13[b]
DBP (mmHg)	86.50 ± 1.09	81.33 ± 0.76[a]	78.67 ± 0.80[b]	76.67 ± 1.17[b]	82.33 ± 1.76	79.17 ± 1.35
MAP (mmHg)	96.50 ± 1.06	93.17 ± 0.70[a]	86.67 ± 1.23[b]	86.83 ± 0.83[b]	90.33 ± 1.38[b]	88.67 ± 1.09[b]
PP (mmHg)	29.00 ± 1.46	34.33 ± 0.99[a]	23.83 ± 1.68[b]	29.8 ± 1.54[a,b]	23.83 ± 1.45[b]	28.00 ± 3.76

Data are presented as mean ± SEM.
[a] $P < 0.05$, comparison between male and female mice within the same strain.
[b] $P < 0.05$, significant differences relative to the corresponding sex in BALB/c mice.
[c] $P < 0.05$, significant differences relative to the corresponding sex in C57BL/6J mice.
HR = heart rate, SBP = systolic blood pressure, DBP = diastolic blood pressure, MAP = mean arterial pressure, PP = pulse pressure.

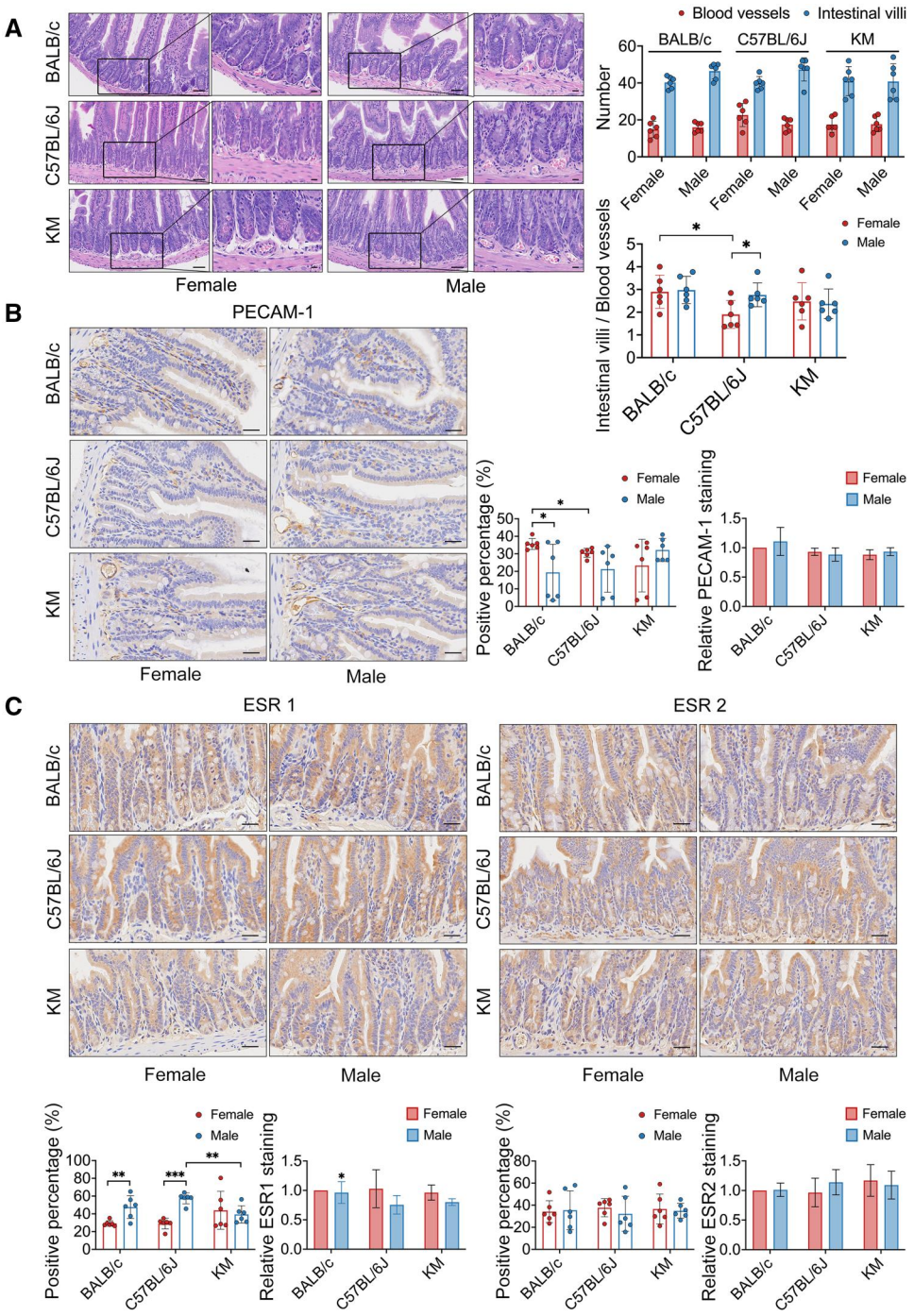

Figure 1. Hematoxylin and eosin (HE) staining and immunolabeling analysis of intestinal tissue from BALB/c, C57BL/6J, and KM mice. (A) HE staining of intestinal tissue sections revealing morphological details. (B and C) Semi-quantitative assessment of PECAM-1, ESR1, and ESR2 protein expression in intestinal tissues. The analysis includes the percentage of positive cells within high-power fields and the relative staining intensity, normalized to female BALB/c mice. Scale bar = 10 μm. *$P < 0.05$; **$P < 0.01$; ***$P < 0.001$.

significantly between groups, indicating a uniform expression across strains and sexes ($P > 0.05$ for all comparisons).

Strain- and sex-specific patterns of intestinal microvascular blood perfusion

LDF analysis highlighted distinct patterns of microcirculatory blood perfusion across different mouse strains and sexes. Notably, female BALB/c and C57BL/6J mice, in addition to male KM mice, demonstrated consistently high levels of blood perfusion and distribution. In contrast, male BALB/c and C57BL/6J mice, as well as female KM mice, exhibited comparatively lower perfusion rates (Figure 2A). To further dissect these observations, we employed wavelet analysis to scrutinize the physiological activities within characteristic frequency bands that regulate microcirculatory perfusion. This analysis revealed differences in microvascular perfusion signals across sexes and strains, as evidenced by distinct 2D spectra and 3D time–frequency spectral scalograms (Figure 2B and C). Specifically, male BALB/c mice displayed peak activity within the cardiac frequency

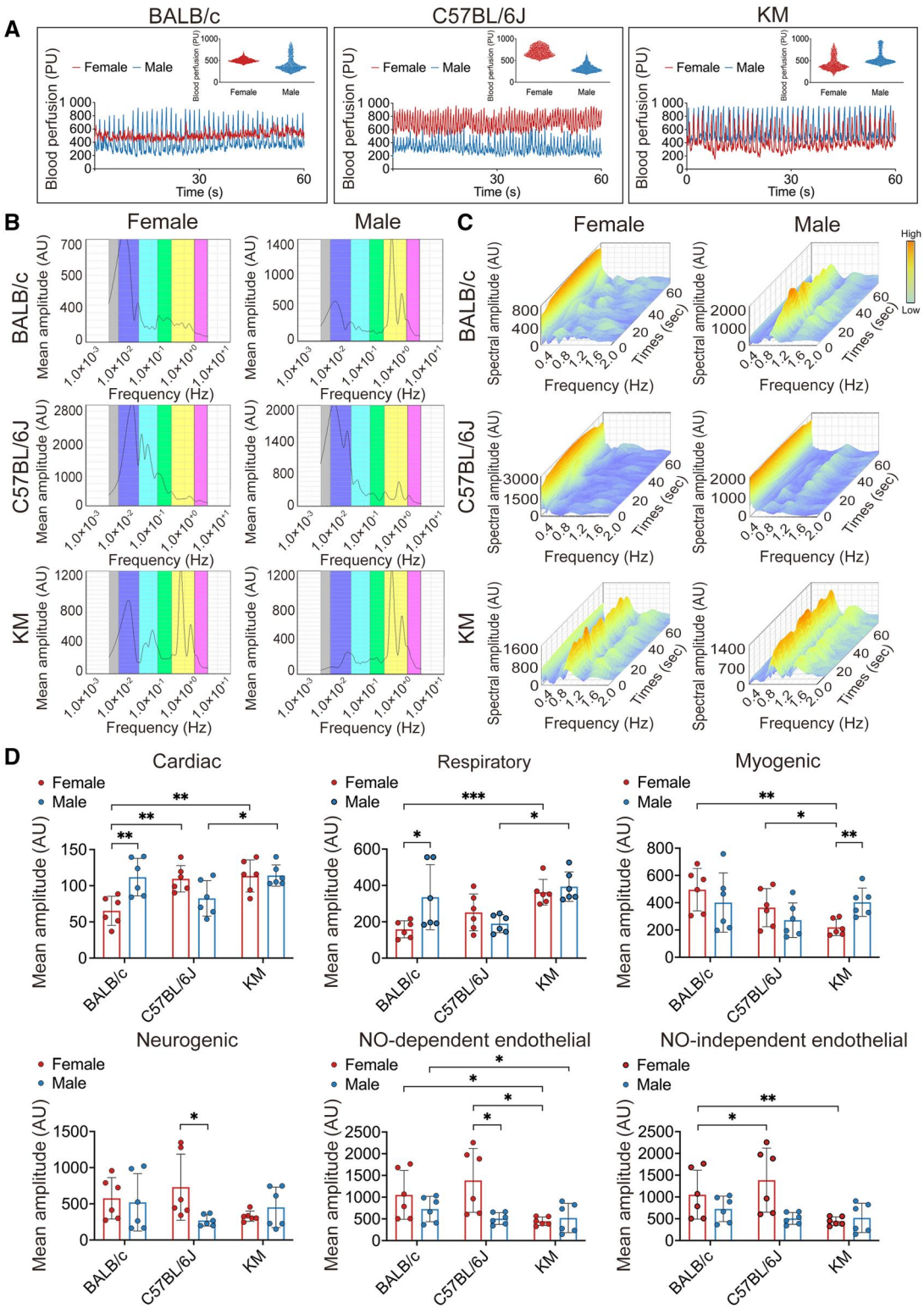

Figure 2. Comparative analysis of intestinal microcirculatory blood perfusion and characteristic oscillatory amplitudes in different mouse strains. (A) Microcirculatory blood perfusion patterns in BALB/c, C57BL/6J, and KM mouse strains. The rectangular insert highlights the extracted pattern of microcirculatory blood distribution. PU = perfusion unit. (B and C) 2D and 3D spectral scalograms representing the characteristic amplitude of intestinal microcirculation profiles. (D) Quantitative analyses of characteristic oscillatory amplitudes in intestinal microcirculatory blood perfusion profiles. $^{*}P < 0.05$; $^{**}P < 0.01$; $^{***}P < 0.001$.

band (0.6–2.0 Hz) whereas the activity of female BALB/c mice peaked in the endothelial cell-derived NO-independent frequency band (0.005–0.0095 Hz). Differing from both, the peak values for the C57BL/6J and KM strains occurred primarily in the endothelial cell-derived NO-independent and cardiac segments, respectively, with the exception of male C57BL/6J mice.

Further quantitative analysis of these perfusion signals (Figure 2D) revealed that both sexes of KM mice exhibited greater amplitudes in the cardiac spectrum than female BALB/c ($P < 0.01$) and male C57BL/6J ($P < 0.05$) mice. Compared with both C57BL/6J females ($P < 0.01$) and their male counterparts ($P < 0.05$), BALB/c females presented significantly lower amplitudes. In the respiratory spectrum, both male and female KM mice showed greater amplitudes than did their C57BL/6J and BALB/c counterparts ($P < 0.05$ for males; $P < 0.001$ for females). Additionally, strain-specific sex differences were observed in BALB/c mice ($P < 0.05$). Conversely, within the myogenic spectrum, the KM females displayed significantly lower amplitudes compared with the other strains ($P < 0.01$ for BALB/c; $P < 0.05$ for C57BL/6J) and KM males ($P < 0.01$). Neurogenic spectrum analysis showed that sex-related differences were only significant in C57BL/6J mice ($P < 0.05$), with no inter-strain difference observed. In the NO-dependent endothelial spectrum, KM mice showed the lowest amplitude, which was significantly lower than that of both male and female BALB/c and female C57BL/6J mice (all $P < 0.05$). In addition, distinct sex-related differences were noted among the C57BL/6J mice ($P < 0.05$). Finally, in the NO-independent endothelial spectrum, BALB/c females exhibited significantly lower amplitudes than C57BL/6J and KM females ($P < 0.05$ and $P < 0.01$, respectively), confirming the complex interplay of strain and sex in the regulation of intestinal microvascular perfusion.

Sex- and strain-related differences in intestinal microvascular blood flow velocities

Our investigations into relative velocity, reflecting microvascular autoregulatory dynamics, revealed distinct patterns across sexes and strains. Female BALB/c and C57BL/6J mice exhibited elevated microvascular autoregulatory blood flow velocities in comparison with their male counterparts. In contrast, velocity measurements between male and female KM mice did not show significant differences (Figure 3A). Wavelet transform analysis elucidated a consistent pattern in the distribution of peak velocities within the intestinal velocity signal spectra across different groups, with the highest peaks predominantly observed in the respiratory amplitude. This pattern was prominent in female mice, which consistently demonstrated higher relative velocity peaks compared with males within the same strain (Figure 3B). Additionally, 3D time–frequency mapping provided further insight into the temporal dynamics of these velocity signals, showing more regular patterns of variation in male BALB/c and female C57BL/6J mice (Figure 3C).

Quantitative analysis of these data revealed inter-strain differences. Compared with both BALB/c and C57BL/6J male mice, KM male mice exhibited significantly greater respiratory spectrum amplitudes ($P < 0.05$ for both strains). This trend extended into the neurogenic spectrum, in which KM males also demonstrated a greater amplitude relative to C57BL/6J males ($P < 0.05$). Furthermore, in the NO-independent endothelial spectrum, C57BL/6J male mice showed significantly lower amplitudes than their BALB/c counterparts ($P < 0.05$). Notable sex-specific variation was observed within the C57BL/6 strain, in which females exhibited a greater amplitude in the NO-independent endothelial spectrum than males ($P < 0.05$). Despite these variations, no significant difference in the cardiogenic, myogenic or NO-dependent endothelial spectra were noted across the strains and sexes (Figure 3D). These findings highlight the complex interplay of sex and genetic background in modulating microvascular blood flow velocities.

Differential patterns of erythrocyte aggregation across mouse strains and sexes

Erythrocyte aggregation, which is characterized by the formation of rouleaux or coin-stack structures of separated red blood cells, significantly influences the non-Newtonian properties of blood flow, thereby affecting microhemodynamics [18]. Our analysis revealed distinct patterns of erythrocyte aggregation across different mouse strains and sexes. Specifically, BALB/c males and KM mice exhibited a stable biorhythmic pattern of aggregation that was absent in BALB/c females and C57BL/6J mice. Despite these differences, the degree of erythrocyte aggregation within each mouse strain was generally consistent between the sexes (Figure 4A). The 2D spectrograms and 3D time–frequency plots of erythrocyte aggregation signals further highlighted these differences (Figure 4B and C). The highest signal peaks were predominantly located in the NO-dependent endothelial segment for BALB/c mice. However, for C57BL/6J and KM mice, these peaks occurred mainly in the respiratory segment. These plots also delineated distinct temporal patterns of erythrocyte aggregation across the different mouse strains and sexes, reflecting the complex interplay between genetic background and physiological sex differences.

Quantitative analysis of these signals revealed significant variations within the cardiac spectrum, in which BALB/c males showed greater amplitudes than their female counterparts and C57BL/6J males ($P < 0.01$ for both comparisons). Within the respiratory spectrum, BALB/c males demonstrated greater amplitudes than both BALB/c females ($P < 0.001$) and C57BL/6J males ($P < 0.001$). Furthermore, BALB/c females exhibited lower amplitudes than females of the other two strains ($P < 0.05$ and $P < 0.01$ for C57BL/6J and KM females, respectively). This trend persisted in the myogenic spectrum, in which BALB/c females displayed lower amplitudes than both BALB/c males ($P < 0.001$) and KM females ($P < 0.01$). Moreover, compared with C57BL/6J males, BALB/c males exhibited greater amplitudes across the myogenic, neurogenic, and NO-dependent endothelial spectra (all $P < 0.05$). Significant sex-related differences were also observed within the C57BL/6J strain across these spectra ($P < 0.05$; Figure 4D). These findings highlight the role of genetic and sex differences in modulating erythrocyte aggregation and, consequently, in microhemodynamics.

Stratified microbial diversity and its functional implications across mouse strains

We processed a cumulative total of 1,669,256 high-quality reads from all the samples, each averaging 421.95 bp in length. At a 97% sequence similarity threshold, these were categorized into 8,330 operational taxonomic units (OTUs). The six groups shared 283 identical OTUs and the number of unique OTUs in each group was 424, 467, 457, 537, 424, and 639 (Figure 5A). We assessed α-diversity, incorporating both species richness indices (Chao1 and Observed_species) and species diversity indices (Shannon and PD_whole_tree), across the BALB/C, C57BL/6J, and KM strains, stratified by sex (Figure 5B). In female BALB/c mice, the metrics for Chao1, Observed_species, and PD_whole_tree were greater than those for C57BL/6J mice but fell short of the levels observed in KM mice. This pattern was mirrored in the metrics for BALB/c males compared with those for C57BL/6J males. Interestingly, C57BL/6J female mice exhibited the lowest Shannon index whereas their male counterparts exhibited the lowest PD_whole_tree index. No significant difference in these diversity indices were observed between the sexes within any strain, highlighting variations in the gut microbiome diversity among mice with different genetic backgrounds.

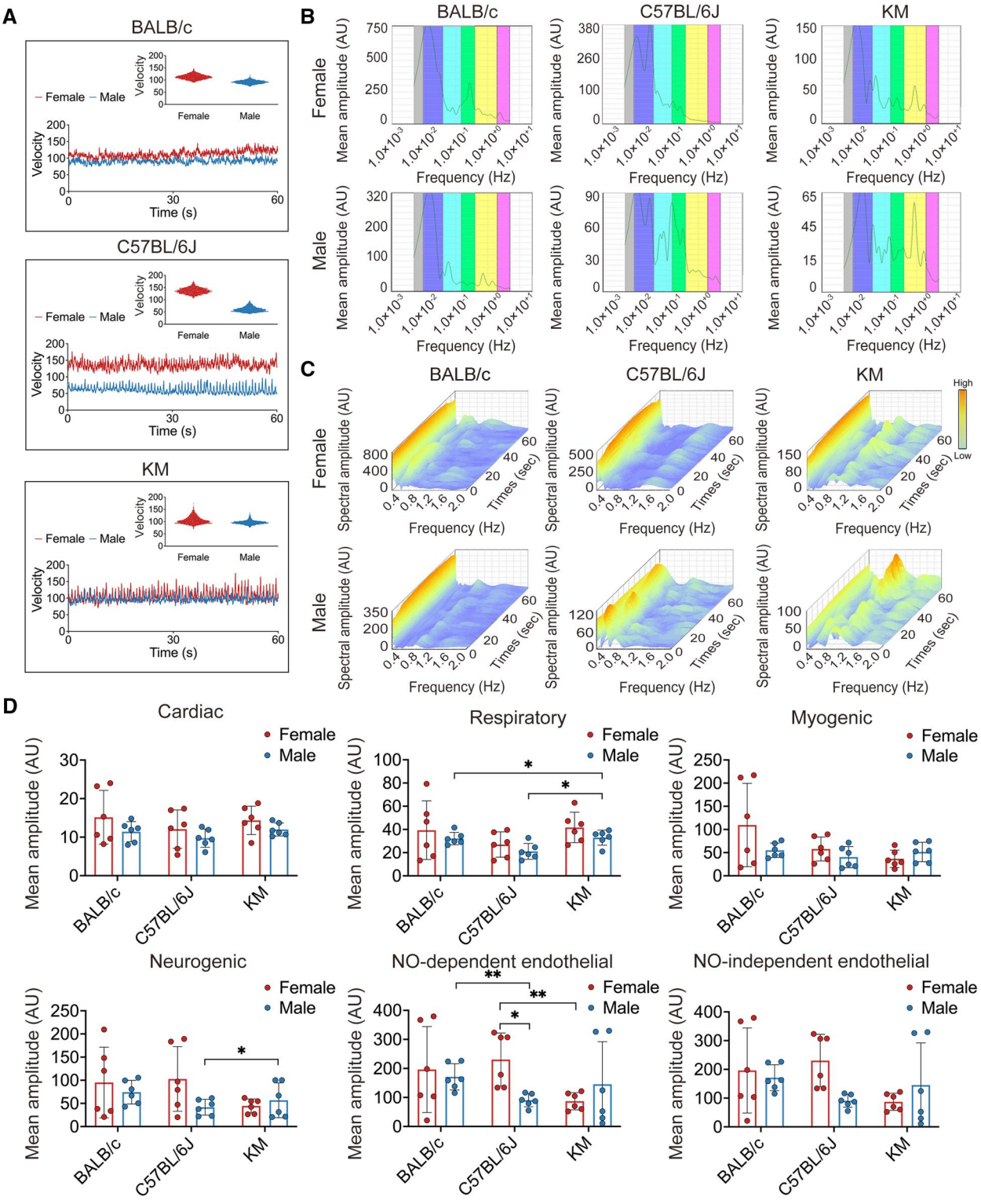

Figure 3. Comparative analysis of intestinal microcirculatory blood flow velocity between BALB/c, C57BL/6J, and KM mice. (A) Measurement of intestinal microcirculatory blood flow velocity in BALB/C, C57BL/6J, and KM mice. The distribution pattern of microcirculatory blood flow velocity is presented in the rectangular insert. (B and C) 2D and3D spectral scalograms illustrate the characteristic amplitude of the intestinal microcirculatory blood flow velocity. (D) Quantitative analysis of the characteristic oscillatory amplitudes from the intestinal microcirculatory blood flow velocity profiles. $^{*}P < 0.05$; $^{**}P < 0.01$; $^{***}P < 0.001$.

β-diversity conducted through principal coordinate analysis and non-metric multidimensional scaling revealed the distinct microbial community compositions among the strains. The microbiome composition of the BALB/C mice diverged significantly from that of the C57BL/6J mice and the variation was less marked in the KM mice (Figure 5C and D). Additionally, a sex-related bifurcation in the microbiota structure was observed predominantly in C57BL/6J mice. Analysis of similarities confirmed that these differences were statistically significant (Supplementary Table S1), suggesting inherent differences in bacterial composition between the three strains.

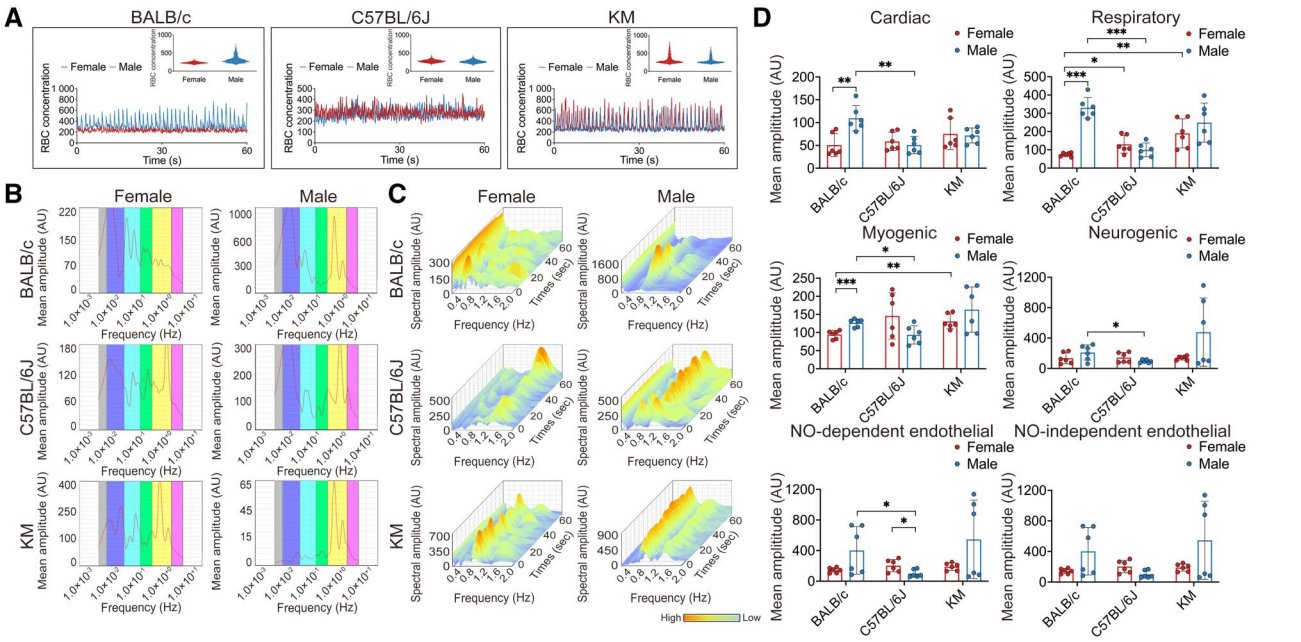

Figure 4. Comparative analysis of intestinal microcirculatory erythrocyte aggregation in BALB/c, C57BL/6J, and KM mice. (A) Intestinal microcirculatory erythrocyte aggregation in BALB/c, C57BL/6J, and KM mouse strains. The rectangular insert provides a detailed view of the erythrocyte concentration distribution pattern. (B and C) 2D and 3D spectral scalograms demonstrating the characteristic amplitude of intestinal microcirculatory erythrocyte aggregation. (D) Quantitative analysis of the characteristic oscillatory amplitudes of intestinal microcirculatory erythrocyte aggregates. $^{*}P < 0.05$; $^{**}P < 0.01$; $^{***}P < 0.001$.

Taxonomic composition analysis at the phylum and genus levels was performed to further elucidate the microbial profiles (Figure 5E and Supplementary Figure S1A). Compared with those in the other groups, the microbial composition of female C57BL/6J mice differed, with *Bacteroidota* and *Firmicutes* representing the predominant phyla, followed by *Proteobacteria* and *Actinobacteriota*. In contrast, *Muribaculaceae* showed the greatest abundance in the other groups, whereas *Akkermansia* was more abundant in female C57BL/6J mice. Linear discriminant analysis effect size (LEfSe) was performed to identify the bacteria that were most likely responsible for the differences observed (Supplementary Figure S1B). These results indicate that *Desulfobacterota* and *Patescibacteria* were predominantly enriched in male KM mice whereas *Verrucomicrobiota* was significantly associated with female C57BL/6J mice.

To explore the functional potential of these microbial communities, we analysed the Kyoto Encyclopedia of Genes and Genomes (KEGG) pathways (Figure 5F). The analysis revealed that the gut microbiota was primarily involved in metabolic pathways, including those related to amino acid, carbohydrate, cofactor, vitamin, terpenoid, and polyketide biosynthesis. Furthermore, significant enrichment was detected in pathways that were related to cellular processes, genetic information processing, and environmental information processing, indicating the broad functional implications of the gut microbiome in physiology.

Spearman's rank correlation analyses were used to determine the relationships between the top 25 bacterial genera and the parameters of intestinal microhemodynamics (Figure 5G). In female BALB/c mice, a significant positive correlation was found between intestinal microhemodynamic perfusion and velocity, and between intestinal microhemodynamic perfusion and the abundance of the *Rikenellaceae_RC9_gut_group*. However, in male BALB/c mice, microhemodynamic perfusion was positively correlated with *Candidatus_Arthromitus*. Among the C57BL/6J group, a compelling correlation was observed between perfusions and the abundance of *Alloprevotella* and *Alistipes* in females, while the genus *RF39* occurred in males. In KM females, a negative correlation with *Muribaculaceae* and *Bacteroides* contrasted with a positive correlation with *Candidatus_Saccharimonas* and *RF39*, suggesting complex interactions between the microbiota and host vascular function. Erythrocyte aggregation showed distinct microbial associations. Specifically, erythrocyte aggregation was positively correlated with the *Rikenellaceae_RC9_gut_group*, suggesting a beneficial role of this genus in promoting erythrocyte function. Conversely, negative associations with *Muribaculaceae* and *Bacteroides* were revealed whereas positive correlations with *Lactobacillus* and *Ruminococcus* were observed in KM females. These findings indicate that certain bacteria may influence erythrocyte behavior, potentially through metabolic byproducts that affect cell–cell interactions within the bloodstream. Notably, the correlations between the abundance of bacterial genera and the level of blood perfusion and erythrocyte aggregation in the small intestinal microcirculation were similar in KM females. In KM male mice, a robust positive correlation was revealed between microvascular perfusion and *Clostridia_UCG-014*, indicating a specific microbial influence on vascular perfusion. Furthermore, the correlation results between intestinal microhemodynamics oscillatory components and bacterial genera revealed that not only *Clostridia_UCG-014*, but also *Lachnospiraceae_NK4A136_group* and *Rikenellaceae_RC9_gut_group* were involved in the physiological oscillatory spectra of intestinal microhemodynamics, including perfusion, perfusion rate, and erythrocyte aggregation (Supplementary Figure S2). These comprehensive analyses delineate a clear relationship between intestinal microhemodynamics and microbial composition that is significantly influenced by both genetic background and sex.

Alterations in intestinal microhemodynamics induced by antibiotic treatment

To further assess the influence of the gut microbiota on the microcirculation of the small intestine, we performed experiments by utilizing broad-spectrum antibiotics (Abx) to deplete bacterial

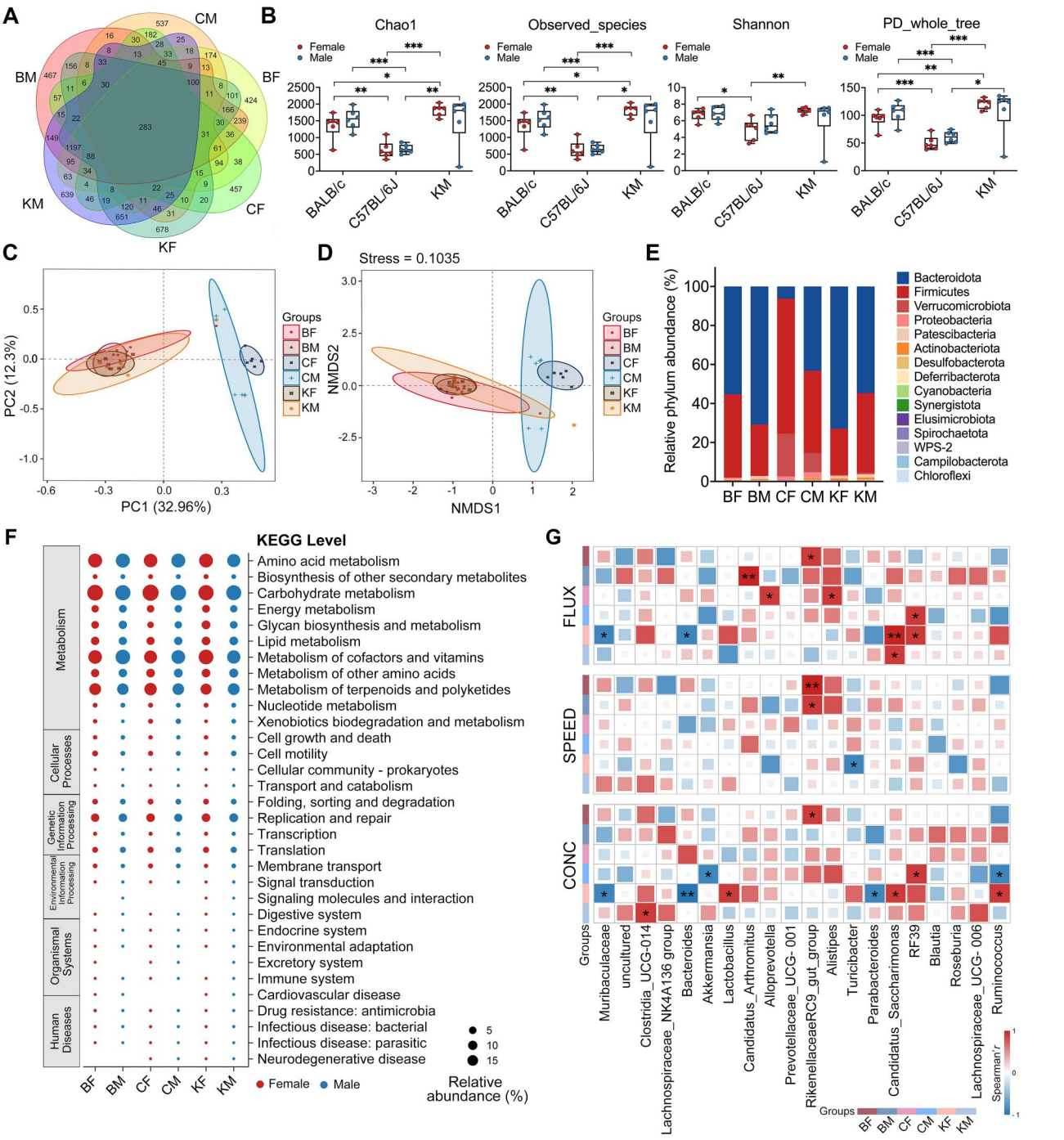

Figure 5. Assessment of the diversity of the gut microbiota in BALB/c, C57BL/6J, and KM mice. (A) Venn diagram illustrating the shared and unique operational taxonomic units (OTUs) among the six groups. (B–D) Alpha and beta diversity analyses depicting the intragroup and intergroup microbial diversity among the six groups, respectively. (E) Bar chart showing the relative abundances of the top 20 microbiomes in BALB/c, C57BL/6J, and KM mice at the phylum level. (F) Bubble chart showing the relative abundances of level 2 KEGG pathways as predicted using PICRUSt2. (G) Heat map displaying the correlation analysis between the dominant bacterial genera and the parameters of intestinal microhemodynamics. BF = BALB/c female, BM = BALB/c male, CF = C57BL/6J female, CM = C57BL/6J male, KF = KM female, KM = KM male. *$P < 0.05$; **$P < 0.01$; ***$P < 0.001$.

populations *in vivo*, enabling the observation of microhemodynamic alterations across different genetically defined mouse strains and sexes. As expected, quantitative analysis of microcirculatory parameters revealed significant alterations in perfusion levels and velocities post-Abx treatment. Specifically, compared with their untreated counterparts, female C57BL/6J mice exhibited a reduction in blood perfusion (Figure 6A). Furthermore, perfusion velocities were consistently decreased across all antibiotic-treated mice, with the exception of male C57BL/6J mice. An increase in erythrocyte aggregation was observed in female BALB/c, male C57BL/6J, and female KM mice following Abx administration.

Wavelet analysis of endothelial function suggested a decrease in NO-dependent endothelial cell amplitudes in Abx-treated female C57BL/6J mice in terms of perfusion levels and velocities, and NO-independent endothelial cell amplitudes in erythrocyte aggregation. C57BL/6J males showed a decrease in both NO-dependent and NO-independent endothelial cell-

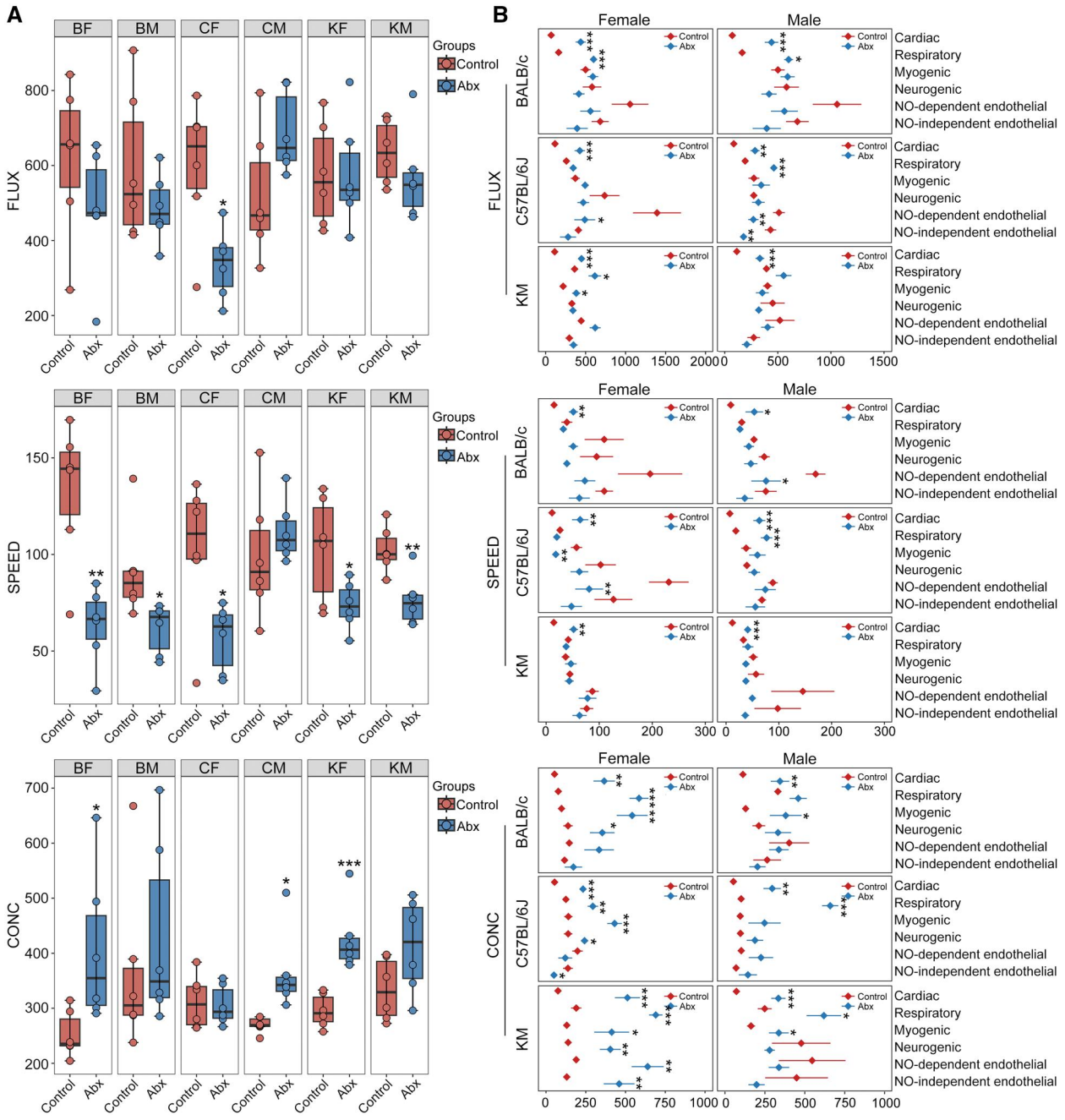

Figure 6. Analysis of intestinal microhemodynamic alterations in Abx-treated mice. (A) Comparative analysis of intestinal microhemodynamics between Abx-treated mice and untreated mice. (B) Analysis of the characteristic oscillatory amplitudes from the intestinal microhemodynamics. BF = BALB/c female, BM = BALB/c male, CF = C57BL/6J female, CM = C57BL/6J male, KF = KM female, KM = KM male. *$P < 0.05$; **$P < 0.01$; ***$P < 0.001$.

derived amplitudes for microvascular blood perfusion whereas KM females showed increased amplitudes for erythrocyte aggregation. An interesting finding was the elevation of cardiac-derived amplitude responses across all antibiotic-treated groups, suggesting a systemic response to gut microbiota depletion that affects cardiovascular dynamics (Figure 6B). The comprehensive dataset (Supplementary Figures S3–S5) highlights the distinct intestinal microhemodynamic responses to antibiotic treatment among different mouse strains and sexes. This finding suggests that both genetic background and sex significantly influence how depletion of the gut microbiota impacts intestinal microcirculation, substantiating the hypothesis that the gut microbiota plays a critical role in regulating intestinal microhemodynamics.

Discussion

The gut microbiota has been increasingly recognized for its significant role in influencing microhemodynamics. The current study revealed that the microhemodynamics of the intestine vary among the BALB/c, C57BL/6J, and KM mouse strains and between the sexes. These variations in intestinal microhemodynamics were associated with distinct gut microbiota compositions. Our results indicated that intestinal microhemodynamic properties, such as microvascular blood perfusion, velocity, and erythrocyte aggregation, exhibit strain- and sex-specific differences in mice, which is consistent with previous reports [19–21]. Our results demonstrate that these physiological variations are closely associated with specific gut microbiota compositions, suggesting a complex interplay

among genetics, sex, and microbial communities in regulating intestinal microcirculation.

The observed variations in intestinal microcirculation observed in this study could be ascribed to a myriad of factors, including the inherent structural and functional adaptability of microvessels to sustained alterations in blood pressure. Furthermore, the influence of sex on the control of microvascular function has emerged as a crucial aspect [22]. The unexpectedly higher percentage of ESR1-reactive cells in male mice compared with females, despite the general association of estrogens with ESR1 upregulation, suggests a multifaceted regulatory interplay involving sexual hormonal and genetic factors. Research indicates that there are significant differences in the expression of various genes and proteins in the intestine between male and female mice, which could influence the expression of ESR1. For instance, a study on the influence of sex on post-resection adaptation in mice found that, although salivary epidermal growth factor levels were lower in females, the adaptive responses in the intestine, such as increases in DNA and protein content, villus height, and crypt depth, were not significantly different between sexes [23]. Additionally, sexually dimorphic gene expression in the intestine of prepubescent mice revealed that several genes, including those linked to intestinal diseases, exhibited sex-specific expression patterns, suggesting underlying epigenetic mechanisms [24]. Another study on the regulation of dihydroxyphenylalanine decarboxylase in the intestine found that male mice displayed higher levels of dihydroxyphenylalanine decarboxylase activity than females, which was dependent on androgens, suggesting a potential link between androgen levels and ESR1 expression [25]. Androgens, which are predominant in males, may upregulate ESR1 expression in the intestine, contrasting with the typical estrogen-mediated pathways observed in other tissues. Additionally, the gut microbiota, which exhibits sex-specific compositions, could modulate local estrogen metabolism and ESR1 expression, further contributing to this divergence. The tissue-specific responses and local regulatory mechanisms within the intestinal microenvironment might also lead to this paradoxical expression pattern. Importantly, higher ESR1 expression in males could enhance estrogenic effects on intestinal microcirculation, improving vasodilation, reducing inflammation, and maintaining microvascular integrity, thus influencing microhemodynamics and disease susceptibility. Estrogens are recognized for their ability to enhance intestinal blood flow through several mechanisms, such as increasing nitric oxide production, reducing the generation of vasoconstrictors, attenuating neutrophil adhesion, and curbing the formation of oxygen free radicals [26, 27]. Sex-related differences in hemorheological properties have also been documented in numerous clinical studies. For instance, compared with male blood, female blood typically exhibits lower viscosity and hematocrit levels, as well as reduced erythrocyte aggregation and enhanced erythrocyte deformability [28].

Wavelet analysis, which facilitates the identification and characterization of non-stationary and intermittent signals, has been used to detect complex physiological signals. The microhemodynamic signals documented in the intestine exhibit a multiscale nature and are influenced by a variety of physiological processes, including cardiac ejection, respiratory cycles, local myogenic activity, and endothelial influences. Previous research has highlighted that disruptions in these oscillatory activities can precipitate a range of pathological conditions, such as hypertension and diabetes [29, 30]. A pivotal discovery in our research was the identification of distinct patterns of oscillatory activities across different mouse strains and sexes. These oscillations, which are indicative of rhythmic contractions and relaxations of the intestinal microvessels, regulate tissue perfusion and oxygenation. Moreover, our study revealed significant correlations between specific oscillatory components and the abundance of certain gut bacterial genera. These correlations suggest a potential interplay between intestinal microhemodynamics and the gut microbiota, highlighting a novel aspect of the gut microvascular axis that warrants further exploration.

The communication between the gut microbiota and intestinal microcirculation suggests potential mechanistic pathways through which microbial diversity influences microvascular health. Dysbiosis, which is characterized by an imbalance in the microbial community, is implicated in the pathogenesis of several vascular disorders, including endothelial dysfunction, hypertension, atherosclerosis, and metabolic syndrome. Key microbial metabolites such as trimethylamine N-oxide (TMAO) and indoxyl sulfate have been identified as modulators of endothelial function. These metabolites impact the vascular system by altering nitric oxide production, influencing the expression of adhesion molecules, and triggering inflammatory responses [31–33]. Furthermore, disruptions in the gut microbiota have been associated with a range of systemic effects including gastro-intestinal disorders, metabolic syndrome, and inflammation. These conditions contribute to microangiopathy and damage to intestinal microvascular endothelial cells, which often result from persistent low-grade inflammation and oxidative stress [34, 35]. The relationship between the gut microbiota and microcirculation is further complicated by the role of sex hormones such as estrogen, which has been shown to promote microbial diversity and influence microvascular health. Our findings indicate that, despite observable differences in microbial colony composition between male and female mice, no significant differences in overall microbial diversity were noted between the sexes. This observation suggested that, although the presence and proportion of specific microbial communities may differ between sexes, the overall complexity and richness of the microbial ecosystem remain constant. This constancy could be crucial for maintaining endothelial health across different physiological conditions. The absence of significant sex-related differences in microbial diversity might also reflect a fundamental resilience of the gut microbiome to variations in hormonal levels that typically distinguish male from female physiology.

In addition, the gut microbiota plays a pivotal role in diverse physiological processes, such as modulating gut motility, nutrient absorption, and the immune response [36], which can subsequently impact intestinal microhemodynamics. Therefore, differences in gut microbiota composition could explain the variations in intestinal microhemodynamics observed among mouse strains and between the sexes. Certain gut commensal bacteria, including *Bacteroides* and *Prevotella*, are known producers of succinate whereas the *Ruminococcus* family is recognized for its butyrate production. These bacteria play a significant role in modulating short-chain fatty acid production, which directly influences systemic circulation. These metabolites have specific functional roles in controlling the vascular system, promoting angiogenesis, and managing blood rheology [37, 38]. Furthermore, studies have shown that supplementation with *Lactobacillus* can promote endothelium-dependent vasodilation by increasing NO bioavailability, mediated via changes in circulating metabolites. This finding supports the concept that certain gut microbiota can influence vascular health and microhemodynamics [39]. Our findings align with previous research indicating

that host genetics and sex hormones can shape the composition of the gut microbiota [40]. Moreover, we identified specific correlations between the gut microbiota and microhemodynamic parameters, potentially suggesting a role for the gut microbiota in modulating intestinal microhemodynamics.

Furthermore, the gut microbiota is a key factor in regulating endothelial cell function and microvascular development, not only in the intestinal mucosa, but also in the microvasculature of distant organs [41]. In the intestine, the presence of gut microbiota and the subsequent activation of innate immune pathways support the formation of detailed capillary networks and lacteals [42]. This process significantly influences the integrity of the gut vascular barrier and the uptake of nutrients. The complexity of the role of microbiota underscores its importance in maintaining gut health and broader systemic processes [43].

Our investigation clarifies the manner in which genetic and sex-specific factors in conjunction with the gut microbiota modulate intestinal microhemodynamics and sheds light on their potential implications in clinical disorders. The governance of blood flow within the intestinal microvascular bed is mediated by contractile elements in capillaries [44]. During acute hemorrhagic events, the microcirculatory blood flow in the jejunal mucosa exhibits stability, suggesting effective autoregulation. In contrast, other regions such as the pancreas are subject to substantial reductions in flow [45]. The oscillatory flow conditions observed during hemorrhagic shock and subsequent resuscitation emphasize the critical role of dynamic flow analysis in devising efficacious treatment protocols [46]. Moreover, hepatic ischemia-reperfusion has been shown to induce profound microvascular alterations in the small intestine that impact functional capillary density, red blood cell velocity, and leukocyte–endothelial interactions, thereby highlighting the systemic nature of ischemic events. This body of evidence suggests the complex interplay between physiological and pathological states that influences intestinal microhemodynamics, revealing the impact of systemic health on local vascular functions and vice versa, and suggesting the need for personalized therapeutic strategies that consider genetic and sex-based differences.

One potential limitation of this study is the lack of functional assays to validate the physiological implications of the observed differences in intestinal microhemodynamics and the gut microbiota. Future studies that incorporate functional assays and metagenomics could provide a more comprehensive understanding of the roles of the gut microbiota and microhemodynamics in health and disease. In conclusion, our study revealed significant strain- and sex-related differences in intestinal microhemodynamics and the gut microbiota in mice. These findings could provide a foundation for further research into the complex interactions among host genetics, sex, microhemodynamics, and microbiota in the context of intestinal physiology and pathophysiology.

Supplementary Data

Supplementary data is available at *Gastroenterology Report* online.

Authors' Contributions

M.L. contributed to the conception and design of the study. Material preparation, data collection, and analysis were performed by S.F., M.X., B.W., B.L., Y.L., Y.W., X.L., H.L., Q.W., X.Z., A. L., and X.Z. The first draft of the manuscript was written by S.F. and M.L. Funding was acquired by M.L. All authors read and approved the final manuscript.

Funding

This work was supported by the CAMS Innovation Fund for Medical Sciences [2022-I2M-1–026], the Beijing Municipal Natural Science Foundation [No. 7212068], and the National Natural Science Foundation of China [No. 81900747].

Acknowledgements

The authors thank Yuhong He (Institute of Microcirculation, Chinese Academy of Medical Sciences & Peking Union Medical College) for her assistance with mice blood pressure measuring.

Conflicts of Interest

All the authors have no conflicts of interest to disclose.

References

1. Ogawa H, Binion DG. Effect of enteric flora on inflammatory and angiogenic mechanisms in human intestinal microvascular endothelial cells. *Front Biosci* 2005;**10**:94–8.
2. Spadoni I, Zagato E, Bertocchi A *et al.* A gut-vascular barrier controls the systemic dissemination of bacteria. *Science* 2015; **350**:830–4.
3. Bohlen HG. Integration of intestinal structure, function, and microvascular regulation. *Microcirculation* 1998;**5**:27–37.
4. Nankervis CA, Reber KM, Nowicki PT. Age-dependent changes in the postnatal intestinal microcirculation. *Microcirculation* 2001;**8**:377–87.
5. Watkins DJ, Besner GE. The role of the intestinal microcirculation in necrotizing enterocolitis. *Semin Pediatr Surg* 2013;**22**:83–7.
6. Koike Y, Li B, Ganji N *et al.* Remote ischemic conditioning counteracts the intestinal damage of necrotizing enterocolitis by improving intestinal microcirculation. *Nat Commun* 2020;**11**:4950.
7. Woitowich NC, Beery A, Woodruff T. A 10-year follow-up study of sex inclusion in the biological sciences. *Elife* 2020;**9**:e56344.
8. Huxley VH, Kemp SS. Sex-specific characteristics of the microcirculation. *Adv Exp Med Biol* 2018;**1065**:307–28.
9. Yoon K, Kim N. Roles of sex hormones and gender in the gut microbiota. *J Neurogastroenterol Motil* 2021;**27**:314–25.
10. Tarracchini C, Alessandri G, Fontana F *et al.* Genetic strategies for sex-biased persistence of gut microbes across human life. *Nat Commun* 2023;**14**:4220.
11. Xu L, Huang G, Cong Y *et al.* Sex-related differences in inflammatory bowel diseases: the potential role of sex hormones. *Inflamm Bowel Dis* 2022;**28**:1766–75.
12. Rustgi SD, Kayal M, Shah SC. Sex-based differences in inflammatory bowel diseases: a review. *Therap Adv Gastroenterol* 2020; **13**:1756284820915043.
13. So SY, Savidge TC. Sex-bias in irritable bowel syndrome: linking steroids to the gut-brain axis. *Front Endocrinol (Lausanne)* 2021; **12**:684096.
14. Abdulhameed YA, McClintock PVE, Stefanovska A. Race-specific differences in the phase coherence between blood flow and oxygenation: a simultaneous NIRS, white light spectroscopy and LDF study. *J Biophotonics* 2020;**13**:e201960131.
15. Fredriksson I, Larsson M, Strömberg T *et al.* Vasomotion analysis of speed resolved perfusion, oxygen saturation, red blood cell

tissue fraction, and vessel diameter: novel microvascular perspectives. *Skin Res Technol* 2022;**28**:142–52.
16. Xu M, Fu S, Wang B *et al.* Evaluation of renal microhemodynamics heterogeneity in different strains and sexes of mice. *Lab Invest* 2024;**104**:102087.
17. Kelly CJ, Zheng L, Campbell EL *et al.* Crosstalk between microbiota-derived short-chain fatty acids and intestinal epithelial HIF augments tissue barrier function. *Cell Host Microbe* 2015;**17**:662–71.
18. Liao Z, Zhang Y, Li Z *et al.* Classification of red blood cell aggregation using empirical wavelet transform analysis of ultrasonic radiofrequency echo signals. *Ultrasonics* 2021;**114**:106419.
19. Hart EC, Joyner MJ, Wallin BG *et al.* Sex, ageing and resting blood pressure: gaining insights from the integrated balance of neural and haemodynamic factors. *J Physiol* 2012;**590**:2069–79.
20. Goldman D, Popel AS. A computational study of the effect of capillary network anastomoses and tortuosity on oxygen transport. *J Theor Biol* 2000;**206**:181–94.
21. Bishop JJ, Nance PR, Popel AS *et al.* Effect of erythrocyte aggregation on velocity profiles in venules. *Am J Physiol Heart Circ Physiol* 2001;**280**:H222–36.
22. Miller VM, Duckles SP. Vascular actions of estrogens: functional implications. *Pharmacol Rev* 2008;**60**:210–41.
23. Stern LE, Falcone RA Jr, Kemp CJ *et al.* Salivary epidermal growth factor and intestinal adaptation in male and female mice. *Am J Physiol Gastrointest Liver Physiol* 2000;**278**:G871–7.
24. Steegenga WT, Mischke M, Lute C *et al.* Sexually dimorphic characteristics of the small intestine and colon of prepubescent C57BL/6 mice. *Biol Sex Differ* 2014;**5**:11.
25. López-Contreras AJ, Galindo JD, López-García C *et al.* Opposite sexual dimorphism of 3,4-dihydroxyphenylalanine decarboxylase in the kidney and small intestine of mice. *J Endocrinol* 2008;**196**:615–24.
26. Vieira RF, Breithaupt-Faloppa AC, Correia CJ *et al.* 17β-Estradiol as a New Therapy to Preserve Microcirculatory Perfusion in Small Bowel Donors. *Transplantation* 2020;**104**:1862–8.
27. Yokoyama Y, Schwacha MG, Bland KI *et al.* Effect of estradiol administration on splanchnic perfusion after trauma-hemorrhage and sepsis. *Curr Opin Crit Care* 2003;**9**:137–42.
28. Bogar L, Juricskay I, Kesmarky G *et al.* Gender differences in hemorheological parameters of coronary artery disease patients. *Clin Hemorheol Microcirc* 2006;**35**:99–103.
29. Stefanovska A, Bracic M, Kvernmo HD. Wavelet analysis of oscillations in the peripheral blood circulation measured by laser Doppler technique. *IEEE Trans Biomed Eng* 1999;**46**:1230–9.
30. Smirni S, McNeilly AD, MacDonald MP *et al.* In-vivo correlations between skin metabolic oscillations and vasomotion in wild-type mice and in a model of oxidative stress. *Sci Rep* 2019;**9**:186.
31. Karbach SH, Schönfelder T, Brandão I *et al.* Gut microbiota promote angiotensin II-induced arterial hypertension and vascular dysfunction. *J Am Heart Assoc* 2016;**5**:e003698.
32. Querio G, Antoniotti S, Geddo F *et al.* Modulation of endothelial function by TMAO, a gut microbiota-derived metabolite. *Int J Mol Sci* 2023;**24**:5806.
33. Amedei A, Morbidelli L. Circulating metabolites originating from gut microbiota control endothelial cell function. *Molecules* 2019;**24**:3992.
34. Zucoloto AZ, Schlechte J, Ignacio A *et al.* Vascular traffic control of neutrophil recruitment to the liver by microbiota-endothelium crosstalk. *Cell Rep* 2023;**42**:112507.
35. Lanik WE, Luke CJ, Nolan LS *et al.* Microfluidic device facilitates in vitro modeling of human neonatal necrotizing enterocolitis-on-a-chip. *JCI Insight* 2023;**8**:e146496.
36. Nicholson JK, Holmes E, Kinross J *et al.* Host-gut microbiota metabolic interactions. *Science* 2012;**336**:1262–7.
37. Kiouptsi K, Pontarollo G, Reinhardt C. Gut microbiota and the microvasculature. *Cold Spring Harb Perspect Med* 2023;**13**:a041179.
38. He Y, Jiang H, Du K *et al.* Exploring the mechanism of Taohong Siwu Decoction on the treatment of blood deficiency and blood stasis syndrome by gut microbiota combined with metabolomics. *Chin Med* 2023;**18**:44.
39. Malik M, Suboc TM, Tyagi S *et al.* Lactobacillus plantarum 299v supplementation improves vascular endothelial function and reduces inflammatory biomarkers in men with stable coronary artery disease. *Circ Res* 2018;**123**:1091–102.
40. Org E, Mehrabian M, Parks BW *et al.* Sex differences and hormonal effects on gut microbiota composition in mice. *Gut Microbes* 2016;**7**:313–22.
41. Khandagale A, Reinhardt C. Gut microbiota—architects of small intestinal capillaries. *Front Biosci (Landmark Ed)* 2018;**23**:752–66.
42. Bayer F, Dremova O, Khuu MP *et al.* The Interplay between Nutrition, Innate Immunity, and the Commensal Microbiota in Adaptive Intestinal Morphogenesis. *Nutrients* 2021;**13**:2198.
43. Meng X, Zhang G, Cao H *et al.* Gut dysbacteriosis and intestinal disease: mechanism and treatment. *J Appl Microbiol* 2020;**129**:787–805.
44. Wille KH, Schnorr B. The occurrence of hemodynamic effective elements in the intestinal blood vessel system [Article in German]. *Anat Histol Embryol* 2003;**32**:94–7.
45. Krejci V, Hiltebrand L, Banic A *et al.* Continuous measurements of microcirculatory blood flow in gastrointestinal organs during acute haemorrhage. *Br J Anaesth* 2000;**84**:468–75.
46. Szabó A, Suki B, Csonka E *et al.* Flow motion in the intestinal villi during hemorrhagic shock: a new method to characterize the microcirculatory changes. *Shock* 2004;**21**:320–8.

Gastroenterology Report, 2024, 12, –
https://doi.org/10.1093/gastro/goae087
Original Article